ON WATER DETECTION IN THE MARTIAN SUBSURFACE USING SOUNDING RADAR

E. HEGGY

Observatoire Astronomique de Bordeaux, BP 89, 33270 Floirac, France

E-mail: heggy@observ.u-bordeaux.fr

P. PAILLOU

Observatoire Astronomique de Bordeaux, BP 89, 33270 Floirac, France

E-mail: paillou@observ.u-bordeaux.fr

G. RUFFIE

PIOM, CNRS UMR 5501, ENSCPB, Talence, France

E-mail: g.ruffie@piom.u-bordeaux.fr

J.M. MALEZIEUX

Institut EGID, Université de Bordeaux III, France

E-mail: jmmalez@egid.u-bordeaux.fr

F. COSTARD

Université Paris-Sud, Orsay, France

E-mail: fcostard@geol.u-psud.fr

G. GRANDJEAN

BRGM, 45060 Orléans, France

E-mail: g.grandjean@brgm.fr

Submitted to ICARUS
7/3/2001
Revised : 2/7/2001
Acctedpted : 13/7/2001

Number of pages: 29
Number of tables: 4
Number of figures: 12

***KEYWORDS**:* Mars, Radar, subsurface, Mineralogy.

ON WATER DETECTION IN THE MARTIAN SUBSURFACE USING SOUNDING RADAR

CONTACT INFORMATIONS

Name:	Essam HEGGY
Address:	2 rue de l'Observatoire, BP 89, 33270 Floirac, France
Email:	heggy@observ.u-bordeaux.fr
Phone:	(33) 5 57 77 61 28
Fax:	(33) 5 57 77 61 10
Occupation:	(1) Bordeaux Astronomical Observatory, France. (2) Astronomy Department, Cairo University, Egypt.

ABSTRACT
Several radar experiments are foreseen to map the Martian subsurface down to several kilometers, searching for subsurface liquid water reservoirs, using different concepts and techniques, all based on the penetration property of the radio frequency waves in arid soils. The penetration depth of low frequency radar is mainly related to the electromagnetic properties of the investigated medium. Thus a good knowledge of the Martian subsurface dielectric profile along the first kilometers is necessary for the future water identification and data interpretation. We have investigated in this work the electrical and magnetic properties of the Martian surface and subsurface, using terrestrial laboratory analogues in the frequency range 1-500 MHz, covering the frequency domain of the Mars Advanced Radar for Subsurface and Ionosphere Sounding (MARSIS) experiment on board the Mars Express mission (ESA–2003), the NetLander Ground Penetrating Radar (GPR) (CNES–2007) and future sounding radar that may be updated to the Mars exploration program in the "Follow the water" strategy. In our approach, we constructed experimentally a most common dielectric profile representative of the Martian subsurface by measuring the electric permittivity and magnetic permeability of well defined mixtures of basaltic, volcanic and sedimentary materials that have been reported for Mars. We also considered iron oxides (hematite and maghemite) and evaporites that may be present such as gypsum, and their mixtures with representative amounts of the Martian geological context under the most common petrophysical and geophysical conditions, along the subsurface profile. This led to synthetic representative samples of the Martian subsurface materials under adequate conditions of porosity and temperature that should exist in the first 2.5 km of the upper crust. Dielectric measurements show that the first layers of the Martian subsurface (few hundreds of meters), which are mainly constituted of volcanic iron rich materials, could dramatically decrease the radar penetration depth initially foreseen, thus limiting deep subsurface exploration. We also investigated the constraints on subsurface water detectability in a radar lossy medium and its dielectric identification among surrounding geological materials.

INTRODUCTION

The surface morphology of Mars attests the past presence of a fluid in the liquid phase, more probably water (Malin and Edgett, 2000a). Due to the low atmospheric pressure of about 6 hPa and the mean surface temperature of 210 K, liquid water could hardly exist now at the surface of Mars. Recent high resolution images from the Mars Orbital Camera (MOC) on board the Mars Global Surveyor (MGS) orbiter reveals the possibility of the presence of water in the near subsurface at a depth of a few hundred meters, outgoing from an underground layer of ground ice (Malin and Edgett, 2000b) covered by volcanic altered materials as shown in Fig.1. Another evidence is the shape and diameter of the rampart craters as in Fig.2, which provides us information about the presence of ice-rich crust and its stability (Costard, 1989, Kuzmin et al., 1988). Theoretical geophysical models (Clifford, 1993) predict that liquid water reservoirs on Mars should be around the 2.5 km depth, where the temperature gradient may reaches the ice fusion point, the fractured ground ice being able to hold liquid water reservoirs.

It is then obvious that, in order to detect this rock-ice / water interface in the Martian subsurface, we need a deep sounding technique. The use of sounding radars seems to be an appropriate tool in terms of mass and energy constraints for planetary space mission (Berthelier et al., 2000). Two space missions will use the low frequency sounding radar technique: the first one is the MARSIS experiment on board of the Mars Express orbiter (ESA-2003), for which the radar will use a high gain antenna to perform vertical sounding from orbit, (Picardi et al., 1999); the other is the Ground Penetrating Radar (GPR) experiment of the NetLander mission (CNES-2007), constituted of four monostatic landers, each one holding identical instruments, including the GPR that will deploy three 35 m monopole antennas and three magnetic antennas (Berthelier et al., 2000). Both systems will operate at frequencies around 2 MHz, searching mainly for deep subsurface water and mapping the geological layered structures and their seasonal variations. Primary calculations of the radar penetration depth considered lunar samples and earth polar regions electrical properties as Martian surface analogues, suggesting the possibility of a penetration depth of 2.5 km for Mars Express, and from 2.5 to 5 km for NetLander. Another future mission is being planned by JPL with the main task to acquire cartography of the whole Martian near subsurface (from 1 to 10 m in depth), using a low frequency P-Band Synthetic Aperture Radar around 330 MHz (Thompson et al., 2000).

In order to evaluate experimentally the performances of such radar systems for Martian applications (and also for arid terrestrial regions), we performed a field survey using a 100 MHz GPR in the Republic of Djibouti, East Africa (Paillou et al., 2001). It is a volcanic and arid region showing a mineralogical and geological context very similar to the one reported by the Mars Pathfinder experiment. Our results showed a non-expected low radar penetration of less than two meters, due to high concentration (about 12 %) of iron oxide materials and evaporites deposits in the dry sedimentary layer that covers the volcanic bedrock. This result led us to the conclusion that the presence of ferromagnetic materials and perhaps evaporites in the Martian sediments, even in low percentages, could dramatically affect the radar penetration depth, and thus screen the deep subsurface exploration foreseen with the 1-500 MHz radars. To study the problem of the radar penetration in the Martian subsurface and take into account the presence of ferromagnetic layers in the first hundreds of meters, we conducted series of measurements of the electromagnetic properties of volcanic and sedimentary materials, in order to construct a most common Martian electric subsurface profile for the 1-500 MHz frequency range. We used expected subsurface physical conditions such as temperature gradient, porosity and granulation that may exist along the first few kilometers of the Martian crust. We divided the Martian subsurface into two main sections: *the near subsurface* and *the deep subsurface*, each constituted of several layers having different geological and mineralogical context, leading to different electrical and magnetic properties. We set up the preparation of our laboratory samples simulating Martian surface and subsurface materials for each geological layer constituting the two partitions, according to the actual knowledge of the Martian surface mineralogy, which is used here as a boundary condition for the subsurface geological and geophysical context.

THE MARTIAN MINERALOGY

The electrical properties of the Martian surface and subsurface layers are strongly related to their mineralogical composition. This information is needed to simulate laboratory representative samples and to experimentally evaluate their electric and magnetic behavior. Mars Pathfinder Advanced Proton X-Ray Spectrometer (APXS) and Viking X-Ray Fluorescence (XRF) in-situ soil chemical analysis showed that iron bearing minerals constitute a large part of the mineral phase of the Martian surface geology. The rock component of the soil

analyses for the three landing sites is of basaltic type (Rieder et al., 1997). Chemically, the Martian soil is probably constituted of weathered basaltic material (Newsom et al., 1999). This result was confirmed by recent data from the Thermal Emission Spectrometer (TES) on board the Mars Global Surveyor (MGS) orbiter and multispectral images of Mars obtained during the Earth – Mars opposition in 1994 and 1998 by the Hubble Space Telescope: they show the presence of isolated regions of crystalline hematite (α-Fe_2O_3) with grain sizes around 50 µm (Bell and Morris, 1998; Christensen et al., 1999; Christensen et al., 2000). In addition, previous observations reported by Viking indicate the presence of highly magnetic minerals, constituting 1% to 7% of surface materials, more likely to be maghemite (γ-Fe_2O_3) (Hargraves et al., 1977). Pathfinder also reported the presence of maghemite in the Martian dust (Hviid et al.,1997). Other infrared observations from Mariner 9 also suggest the presence of isolated basalt regions (Formizano, pers. commun., 2000). Pyroxenes such as augite and pigeonite have also been identified on the Martian surface using IR measurements (Pinet and Chevrel, 1990).
Complementary sources of information for the Martian near subsurface mineralogy are the SNC meteorites, believed to come from impact materials. Mineralogical analysis shows that all subgroups of the SNC contain traces of water-precipitated minerals such as smectite, illite and gypsum, with a minor amount of halite, calcite and hematite (Gooding, 1992). Using an X-ray diffractometer, we analyzed a powder of the Nakhla meteorite and confirmed the basaltic mafic aspect (pyroxenes and olivine have been clearly identified). Most of the SNC also contain traces of volatile compound with retention of residual magmatic volatiles and late stage interactions with aqueous solutions (Gooding, 1992). Thus they can be used to study the electrical properties of water emerged fields. All these observations confirm that the Martian surface is a basaltic altered terrain, with a discontinuity of the distribution of the ferromagnetic materials. Unlike the surface, there is a lack of direct observational data concerning the materials constituting the Martian subsurface, and no direct measurement describes its mineral phase up to now.

SUBSURFACE GEOLOGICAL AND GEOPHYSICAL CONTEXT

The Martian subsurface is believed to be mainly formed of ground ice whose thickness is varying with the latitude, from 2 km at the equator to 6 km near the poles, probably covering a layer saturated by liquid water (Clifford, 1982). This ground ice (permafrost) is locally covered with volcanic and sedimentary materials as shown by the Clifford assumed geological model in Fig.1. Observational evidence of the presence of a subsurface ground ice, and thus possible water reservoirs, is suggested by the smoothed and rounded surface morphology of the high latitude craters ejecta as the one shown in Fig.2, which provides strong evidence of plastic deformation of the subsurface. Recent high resolution images from the Mars Orbital Camera (MOC) also showed runoff flows outgoing from the subsurface as seen in the Fig.1, confirming the recent water presence in the near subsurface. Sounding radars or GPR require a minimum knowledge of the geological medium investigated, in order to invert the radar echoes and identify geological structures, including subsurface water reservoirs. At the present time, the geological and geophysical context of the Martian subsurface is not known enough to properly accomplish this inversion task. We first considered a general geological model of the Martian subsurface, which was our guideline to construct representative laboratory samples for each layer, and then measured their electrical properties under appropriate physical conditions. Figure 3 represents this model of the Martian megaregolith proposed by Clifford in 1993. We classified the Martian subsurface layers according to their electrical conductivity into two main partitions: the near subsurface and the deep subsurface.

SURFACE AND NEAR SUBSURFACE

Ranging from the surface to 400 m in depth, the Martian near subsurface is mainly composed of fractured and altered volcanic materials such as crater ejecta, volcanic flows, weathering and sedimentary products. Most of materials are rich in iron oxides, which constitutes a lossy medium for the radar waves. According to Viking 1/2 and Pathfinder in-situ chemical analysis, Mars surface is believed to be homogeneously dust covered and constituted of a mixture of a relatively conducting phase materials, mainly ferromagnetic minerals such as hematite, maghemite and a relatively insolating phase materials such as silicas and basaltic rocks. Atmospheric measurements suggest that the dust layer is covering nearly all the Martian surface.
This thin layer of a few meters thickness (1 to 10 m) will thus play a major role in the radar ability to penetrate the next layers. To simulate this dust material, we used as a first approximation a non-compacted powder of Djiboutian basalt mixed to a varying mass concentration of hematite and maghemite, at a granulation of 50 µm. The basalt used here looks very similar to the Martians one, as shown in Table I (Paillou et al., 2001). We

performed measurements at a temperature of 230 K, representing the mean temperature of the Martian surface (in the equatorial and near polar regions), and a sample porosity of 50%. The geological model of the Martian subsurface predicts also the presence of a layer of fractured basalt rocks as a result of strong alteration processes at depth ranging from 10 to 50 m. We simulated this layer using a compacted powder of basalt mixed to hematite and maghemite with a mass percentage of 20%. For the third layer in Fig.3, we used a Djiboutian basalt machined pellet to simulate the volcanic bedrock layer from 50 to 200 m in depth. We took a special care for simulating the sedimentary deposits layer ranging from 200 to 400 m in depth: we used a compacted powder of Nakhla SNC meteorite, which contains olivine, pyroxenes and sedimentary materials. We assumed in this approach that the SNC parent planet is Mars and that they contain materials coming from the near subsurface.

DEEP SUBSURFACE

Unlike the geological layers discussed above, the Martian deep subsurface ranging from 400 to 2500 m is supposed to be mainly constituted of ground ice and fractured porous volcanic rocks, where pores and fractures are filled with ice or water depending on the local geothermal stability (Carr, 1996). The amount of ice in the ground ice is depending on the porosity of the rocks. Those materials seem to be less absorbent for the radar waves compared to the first regolith layers. The electrical properties of the Martian deep subsurface are strongly related to the ice thermodynamic stability, which in turn depends on the ice salinity, the geothermal gradient, and the porosity of rocks.
Electrical properties of ice materials are quite well known. Both laboratory measurements (Johari and Charette, 1975) and field investigations (Raymond and England, 1976; Vaughan et al., 1999) prove that such layers present regular and low complex dielectric values in the 5 MHz – 1 GHz frequency range, leading to low attenuation and then deep radar penetration. While the permittivity values of rock-ice materials are more important in the 1 to 100 MHz frequency range and the 245 to 275 K temperature range, they increase linearly with the temperature. To study the electrical properties and the behavior of such geological layers, we used a watertight capacitive cell filled with basalt powder and we added 20% of water. We then put the cell in a cold room to reach the temperature of 230 K. We compacted each sample to reach a porosity of 25%, in order to fit the Martian porosity profile at this depth.
Previous works (Chyba et al., 1998) that discussed the electrical properties of ice mixed components showed that ice, once coupled with ferromagnetic materials, could have an important dielectric complex value and thus increase radar absorption. The thick ground ice layer is also likely to present a local dielectric gradient depending on its geothermal conditions, leading to the existence of an absorption gradient. The depth of the ice-water limit, to be detected with a sounding radars, depends on the Martian geothermal gradient (which is poorly known), the latitude, the salt concentration in ground ice, and the porosity of rocks, since all these parameters control the ice pre-melting effect. We fixed this ice-water transition interface to 2.5 km in Fig.3. Table II summarizes our laboratory sample characteristics with their corresponding geological profile as described in Fig.3.

EXPERIMENTAL SETUP AND SAMPLE PREPARATION

In the current section, we will describe briefly our experimental procedure, which is necessary to evaluate the source and amount of errors in each series of measurements.
The measurement of the electromagnetic properties of volcanic materials as a function of the Martian geothermal gradient and porosity profile for the 1-500 MHz frequency range is a quite complex task. We have to deal with high conductivity values in the Radio frequency domain, and instrumental constraints for low temperature permittivity and permeability measurements using capacitive cells require several precautions to avoid moisture deposit inside the sample or on its surface. We also have to consider the contribution of the granulation size parameter, and precautions in sample preparation in order to avoid an abnormal dielectric behaviour due to unsymmetrical pellets (bad surface contacts in the measuring cell).

INSTRUMENTATION

To perform permittivity measurements we have used two capacitive cells specially designed in order to avoid the resonance that occurs in classical capacitive cells, due to radio frequency interaction with conducting materials. The first one is noted by (a) in Fig.4, in this cell we used machined and compacted pellet. The second

one noted by (b) in Fig.4 is an open coaxial cell used to measure the dielectric constant of powder-reduced material. Both of the two dielectric cells were connected to the HP4192A analyser to perform the measurements in the frequency range 1 to 10 MHz. A second HP4291A analyser was used to cover a wider frequency range up to 500 MHz. The use of the two analysers avoids measurements in the limits of each frequency band where error exceeds 3%. Both analysers were connected to a central command unit to extract data and calculate in real-time the real and imaginary part of the complex dielectric constant ($\varepsilon = \varepsilon' - i\varepsilon''$) and magnetic permeability ($\mu = \mu' - i\mu''$). For the low temperature measurements, we connected a liquid nitrogen circuit to the cells to keep the samples dry and cold during the measure, and avoid water vapour condensation. We measured several time the permittivity and permeability of each sample to make sure it remains constant over the time of measurement.
Samples permeabilities were evaluated using the magnetic cell HP16454A noted by (c) in Fig.4, connected to both analyser described above. Unlike the electrical cells we were only able to use reduced powder material, due to difficulties to perform rock machined and powder compacted samples having toric form to fit the cell cavity.
Porosity measurement on compacted samples were done using a mercury porosimeter (Autopore III by Micrometrics), with two pressure cycles in order to evaluate small and large pores. Those measurements allowed us to verify also the Gaussian distribution of the grain size inside the compacted samples, and detect the presence of fine fractures inside the samples that could produce resonance during the electromagnetic characterization.

SAMPLE PREPARATION

Rocks samples of hematite, maghemite, Djiboutian basalt, calcite and gypsum were first washed with pure water to minimise any dust contamination and then dried in a heater at a temperature of 350 K for two days in order to remove moisture inside the sample. X-ray analysis was performed to ensure mineralogical composition for each sample. A part of the rock sample was machined into pellets, while the other part was reduced to powder with a controlled granulation of 50 µm. From powder materials, we made pressed pellets with a controlled compaction in order to simulate the Martian porosity profile and study the effect of porosity variation on the permittivity. We also used pure silica powder (50 µm grains) to calibrate our permittivity measurement process. We mixed one-phase minerals and Djiboutian basalt to produce more complex samples, presenting chemical and mineralogical constitution close to the ones reported from the Viking and Pathfinder instruments. Once all the samples were in their final state, they were kept once again for 48 hours in the heater, since even a small amount of moisture can dramatically affect the permittivity measurement (giving higher complex dielectric values than the expected ones).
We fixed the grain size of all samples to 50 µm in order to avoid variations of the electric and magnetic behaviour related to granulation. The change in grain size appears to be important for the permittivity of hematite (Gomaa et al., 2000) and the magnetic permeability of maghemite (Hviid et al., 1997), and could conduct to higher values than the one presented in the next section. The same process was used to build samples of the Martian subsurface under adequate varying compaction levels, using a hydraulic press. The compaction was derived by computing the mean Martian lithosphere pressure for each layer depth using Equation 1, knowing the mean density of the Martian crust and its gravitational constant as the following:

$$\rho_{Mars}\, g_{Mars}\, d = M_{hyd}\, g_{earth} / A_{pastilles} \qquad (1)$$

Where $A_{pellets}$ is the pellet surface area, g_{earth} and g_{Mars} are the gravitational constant of the Earth and Mars respectively, d is the layer depth in the Martian subsurface, M_{hyd} is the mass applied to compact the samples, and ρ_{Mars} is the mean Martian density. Pellets are all 12 mm in diameter and about 2 mm in thickness with very smooth parallel surfaces to minimize the resonance errors in the capacitive cell.
The effects of two parameters have been investigated. One concerns low temperature measurements for which samples have been brought down to the temperature of 230 K, in order to study the temperature impact on the permittivity and permeability of Martian analogues. The other concerns the porosity (compaction) effect on the behavior of the dielectric profile for our frequency range. The graph in Fig.5 describes the chart of our measurement procedure for each of the samples presented in Table II, and for different values of temperature and porosity.

RESULTS

Electric and magnetic properties of the volcanic materials are mainly governed by the amount of iron oxides present in mass percentage and its oxidation state. Figure.6 shows the permittivity measurements for a non-compacted powder (porosity of 50% corresponding to a bulk density $\rho = 2.7$ g/cm^3) of hematite, maghemite, basalt and silica. Measurements were performed using the open cell in the frequency range 1-10 MHz and for a temperature of 230 K. We obtain a relatively low value for the real part of the dielectric constant, mainly due to the high porosity, while the imaginary part is relatively high, except for silica used here as a reference value. Samples in Fig.6 are presented with an increasing value of FeO mass percentage, starting from silica, which contains no iron oxide, to maghemite and hematite. For Djiboutian basalt and silica, the real part of the dielectric constant does not show a significant frequency dependency on this narrow frequency range, due to their low concentration in iron oxide. For hematite and maghematite, we noted an important (quite exponential) dependency of the two curves around 1 MHz. This behaviour concerns also the imaginary part of the dielectric constant (specially for maghemite), which mainly characterise the absorption of the material.

Measurements performed on compacted samples that simulate the subsurface materials are shown in Fig.7. We show that volcanic materials, once compacted (porosity between 20% and 30%), present a high dielectric constant. We can also note in Fig.7 that the real part of the dielectric constant remains constant along the frequency range, while the imaginary part for the basalt mixture with hematite and maghemite increases as the frequency decreases. We can deduce that the loss tangent ($\mathrm{tg}\ \delta = \varepsilon'' / \varepsilon'$) for those materials increases as the frequency decreases to 1 MHz.

Table III shows the small variation of ε' and ε'' in the temperature range from 230 to 300 K for powder samples at the 2 MHz frequency. The motion of the bounded charges inside the medium characterizes the permittivity, producing a temporal redistribution under the interaction between the medium and the electric field of the radar wave. The effect of a low temperature on the permittivity is then to slightly decrease (depending on materials and on the temperature gradient) the real part of the complex dielectric constant as shown in Table III: low temperature tends to damp the vibrational motion of dipoles inside the rock, decreasing thus its ability to interact with the wave of the electrical field.

Fig.8 shows that the permittivity (both real and imaginary parts) of the Djiboutian basalt decreases exponentially as the porosity increases. This can be explained by a higher density (lower void content) when porosity decreases. Our experiments showed that the porosity effect has a much more important impact on the electrical properties than the effect of temperature for dry geological materials (Heggy et al., 2000), excepted of course for sample containing water.

Table IV summarizes the permittivity values for the subsurface model presented in Fig.3 at a frequency of 2 MHz (the one foreseen for Mars Express and NetLander radars). Our laboratory samples appear to be more conductive than the values previously proposed (Ori and Ogliani, 1996; Picardi et al., 1999), since authors did not take into account the compaction effect, and one can hardly find measurements at 2MHz in the literature: values for the dielectric constants that have been used to estimate the radar penetration depth have been extracted from measurement in the 100 MHz – 1 GHz frequency range, and then extrapolated to the 1 – 10 MHz range. We show in particular that larger loss tangent should be considered for the 2 MHz sounding radars, leading to higher attenuation values.

In our experiments, the primary source of errors was the pellet thickness (2 mm) that can produce resonance peaks in the permittivity-frequency curve for frequencies higher than 100 MHz. We carried out our experiments to the limiting frequency of 500 MHz, but this frequency range is not relevant to study deep subsurface layers, since the penetration depth becomes too small in that case. However, we can confirm that a 330 MHz imaging SAR as the one foreseen by JPL (Thompson et al., 2000) should be able to penetrate at least 10 meters of Martian dust.

As a main task of our experiments was to study the subsurface water detectability, Table IV presents the permittivity measurement for wet basalt (20% H_2O) that clearly shows an important dielectric contrast with the upper ground ice layer. Mixtures containing water have a high permittivity that is attributed to the strong polarimetric dissymmetry of the H_2O molecule. All geological materials present a decreasing value of ε' and ε'' as the frequency increases, except for water saturated media that have a relaxation frequency around 20 GHz (water saturated samples show a slowly increasing slope for the permittivity curve at higher frequencies). Further considerations about water detection are presented in the next chapter.

Magnetic properties of rocks are classified into three classes: diamagnetism, paramagnetism and ferromagnetism. Only the last one can significantly change the complex magnetic permeability value in our frequency range. The rock permeability is governed by the presence of ferromagnetic materials (Olhoeft and Capron, 1994). Permeability measurements presented in Fig.9 were performed with the magnetic cell on powder of hematite and maghemite. They show a significant frequency dependency and a strong increase of the μ' and μ" values below 2 MHz. We must then take into account the absorption due to magnetic relaxations for the Martian dust layer, which could contain both hematite and maghemite. No detectable magnetic properties could be noticed within our instrumental sensitivity and error range for the dry Djiboutian basalt. Since the permeability is a function of the grain size, it is important to note that the magnetic properties discussed above are valid for an average grain size of 50 μm. It was not possible to study the effect of porosity and temperature on the magnetic properties of our samples due to instrumental constraints (difficulties to build samples with a toroid form).

IMPACT ON WATER DETECTION

Despite the simplicity of our approach, our results show a complex wave interaction with the Martian surface and subsurface analogues. Radar sounding performances are generally related to three surface and subsurface parameters: 1) the surface and layer interface slope (i.e. the surface and subsurface geometry), 2) the surface and layer interface roughness and 3) the dielectric properties of the geological materials. If we assume the sounding to be done on a plane terrain, then for the 2 MHz Ground Penetrating Radars on board NetLander and the orbiting radar sounder on board Mars Express, the surface interfaces can be assumed to be smooth according to the first order approximation of the Rayleigh criterion: for a wavelength λ = 150m (in vacuum) and a vertical sounding (incidence angle θ = 0), the standard deviation for a random surface height σ should be:

$$\sigma < \frac{\lambda_{vacuum}}{8\cos\theta} = 18.75\ \mathrm{m} \qquad (2)$$

If we consider the hypothesis that the interfaces between the Martian subsurface layer are also smooth (compared to the wavelength in the subsurface $\lambda_{subsurface} = \frac{\lambda_{vacuum}}{\sqrt{\varepsilon}}$, then $\sigma_{subsurface} = 6.25$ for a mean permittivity ε = 9) and parallel, according to the observed stratigraphy on the exposed wall rock of Valles Marineris (McEwen et al., 1999), Thus the main factor governing the detection of water reservoirs is the electrical behavior of the geological layers covering it. Water detectability with radar is conditioned by two main factors: the ability of radar waves to penetrate down to the depth of the ground ice / liquid water interface, which is supposed to vary between 2 and 6 km (Carr, 1996), and the strength of the dielectric contrast between the ground ice and the wet megaregolith layer containing the water reservoir. As a first order approximation we used a propagative model to evaluate the penetration depth to this interface, thus we will not take in consideration in this paper the volume scattering that tend to decrease significantly the penetration depth. This last feature will be treated in detail in future work. Equation 3 (Ulaby et al., 1982) defines the radar penetration depth δ_p, where J is the attenuation factor (cf. Paillou et al., 2001). We took J=100 for the MARSIS experiment (corresponding to an attenuation of 60 dB) and J=1000 for the NetLander GPR (corresponding to an attenuation of 90 dB). For a given frequency f, this penetration depth is only a function of the permittivity and permeability (where μ in equation 3 is defined as $\mu = \sqrt{\mu'^2 + \mu''^2}$) of each of the geological layer along the wave propagation line.

$$\delta_p = \frac{\ln(J)c}{4\pi f}\left\{\frac{\mu\varepsilon'}{2}\left[\sqrt{1+\left(\frac{\varepsilon''}{\varepsilon'}\right)^2}-1\right]\right\}^{-1/2} \qquad (3)$$

Using our permittivity and permeability measurements, we calculated the penetration depth δ_p in meters and the absorption coefficient α (for the one way propagation) in dB per meter as described in Equation 4 (cf. Table IV) as a function of the frequency for various volcanic samples, to get a first order results about the performance of low frequency sounding radars in a Martian context.

$$\alpha = \frac{2\pi f}{c}\sqrt{\frac{\mu\varepsilon'}{2}\left[\sqrt{1+\left(\frac{\varepsilon'}{\varepsilon''}\right)^2}-1\right]} \quad (4)$$

Fig.10 shows the penetration depth for *J*=100, as a function of the frequency, for representative samples of the Martian assumed surface and subsurface materials. None of the considered materials gives a penetration depth higher than 1.7 km for the 2 MHz frequency. Since the permittivity of the geological layers is a function of their porosity as previously derived from the permittivity measurements presented in Fig.8, we evaluated the penetration depth in Fig.11 as a function of the porosity for the Djiboutian basalt at 2 MHz. We can note from Fig.11 that a 2 MHz sounding radar can hardly achieve a penetration depth of 2.5 km in basaltic material within the possible porosity range of the Martian subsurface: in a volcanic context, penetration depths larger than one kilometer will be very hard to achieve at 2 MHz under the actual hypothesis for the Martian subsurface geology. The computation of the absorption coefficient α in Table IV, shows that the first three layers of the Martian soil, mainly constituted of iron rich materials, are lossy media for the radar frequencies planned to be used for NetLander and Mars Express missions. These layers, down to 200 meters, are more absorbent than expected due to the presence of iron oxide rich minerals such as hematite and maghemite, even at low concentrations. Recent data from the Mars Global Surveyor (MGS) Thermal Emission Spectrometer (TES) show a region interpreted as crystalline hematite, approximately 300 km in diameter, near the equator at ~5°W (Christensen et al., 2000): such regions seem non suitable for radar subsurface investigations.

The second factor to discuss for water detectability is the type of dielectric contrast between ground ice and the wet megaregolith, i.e. we need a sharp ice-water transition compared to the radar wavelength at the interface between the frozen soil and the wet regions. The pores of a frozen soil (ground ice) are likely to contain amounts of unfrozen water at temperatures below 0°C (Anderson and Morgenstern, 1973). This amount of unfrozen water W_u (mass percentage of water) is represented for most remoulded frozen soils by a simple power law equation (Anderson and Tice, 1972):

$$W_u = mT^n \quad (5)$$

Where m and n are experimental characteristic soil parameters, and T is the temperature in degrees Celsius below freezing, expressed as a positive number.

The presence of unfrozen water in ground ice layers implies then the presence of a moisture gradient, leading to a local vertical permittivity gradient near the ground ice / water interface. This gradient can be expanded since it has been proven experimentally that the unfrozen water can move through the frozen soil under osmotic, electrical and thermal gradients (Konrad and Duquennoi, 1993).

Using Equation 5, we calculated the amount of unfrozen water in frozen basalt (*m*=4.81 and *n*=-0.33). Results are shown in Fig.12 for different temperatures. We can note the presence of 3% of liquid water (a value that produces significant changes in the dielectric constant of the ground ice) inside the rock as we reach the –5°C temperature. If we consider the Martian geothermal gradient to be ΔT = -10°C km $^{-1}$ (Clifford, 1993), this gives us a moisture gradient which spreads over at least 500 m, more than one hundred times the sounding radar wavelength at this depth. This small moisture percentage should produce a considerable effect on the dielectric profile by increasing gradually the real and imaginary part of the ground ice layer before reaching the water interface. Thus the ground ice / water interface would not appear on the radar echoes as a sharp peak as expected, but rather it would produce a broad flattened low amplitude peak in the time-backscattered power diagram. Even if this last discussed feature seems to limit the penetration depth for deep water detection, it could be used to differentiate an ice / water interface from other dielectric contrasts due to the presence of a layer of strong conductive materials (e.g. evaporites and clays) among other geological materials. We believe that all the electromagnetic characteristics of the Martian subsurface reported here are acceptable values, but they are not fully representative for the real Martian case, which is certainly more complex. We did not consider so far other effects, such as the UV exposure effect on the electrical properties of the dust layer (Olhoeft, 1991), the locally charged terrains in places where storms occur, and the probable presence of evaporites (halite, gypsum) and clays in the Martian soil. Such materials, if present in the subsurface, are also lossy media (Olhoeft, 1998) that could present dielectric contrast with the surrounding medium and thus could be misinterpreted as water reservoir in the radar profiles.

CONCLUSION

Laboratory dielectric measurement of synthetic analogues of the Martian soil is an important task to accomplish for the future interpretation of the radar data that will be produced by Mars Express and NetLander on board radars. It is also crucial for the design of future radar experiments that will take place within the Mars exploration program as the Shallow Subsurface Sounding Radar (Beaty et al, 2001) foreseen in 2005 on board the Mars Reconnaissance Orbiter (MRO). Radar detection of subsurface water is an important scientific objective that is related to our knowledge of the dielectric profile of the investigated subsurface. We showed, using an experimental procedure, that electrical properties of the Martian subsurface are different from the values previously used to evaluate the penetration depth of sounding radars operating at Radio frequencies. In particular, we measured a higher loss tangent, leading to a much higher attenuation of the radar signal. We also evaluated the effects of the rock porosity and temperature on the dielectric constant of volcanic materials. We deduced from our measurements that the first iron oxide rich layers of the Martian subsurface could strongly attenuate the radar signal, depending on the layer mineralogy and thickness. Ground ice layers could also present abnormal electrical behavior in the presence of a moisture gradient, depending on the subsurface geothermal conditions and porosity of rocks. Our work shows a limitation in the penetration depth to about 1 km (at 2MHz), and a possible absence of a strong dielectric contrast characterizing the ice / water transition. The presence of water reservoirs in a shallow depth does not guaranty their detection and vice versa: deep-water reservoirs could be detectable if the geoelectrical context is favorable at the frequency of sounding (e.g. covering layers constituted by carbonates, which are weak absorbent). Assuming the validity of our geo-electrical model of the Martian subsurface, water in the Martian crust cannot be easily detected for the major part of the Martian volcanic terrains using a frequency around 2 MHz. We should consider specific sites presenting a sharp ice / water transition, and optimize the choice of the sounding frequency to get a satisfying penetration depth versus resolution in order to detect geological evidence of water presence and its evolution in the subsurface. Those results should in particular be taken into account in the choice of the future landing sites of the four NetLander radars. Future work will treat a variety of specific sites of the Martian surface, for which we will construct dielectric models of the subsurface. We shall then simulate radar profiles for each case using the Finite Difference Time Domain (FDTD) method, in order to support the selection of optimal landing sites. Finally, we shall evaluate the potentials of different frequency ranges and polarizations to optimize the instrumental performances of future Martian radars.

ACKNOWLEDGEMENTS

The authors would like to acknowledge the support of J.P. Parneix, B. Spiteri, R. Burlot and A. Cerepi for the all the measurement facilities, and N. Mangold for helpful discussions. We also thank A. Barakat from the Egyptian Geological Museum for providing the Nakhla powder. This research was supported by the French CNRS and is a part of the NetLander development work within the CNES Mars exploration program.

REFERENCES

Anderson, D.M. and N.R. Morgenstern 1973. Physics, chemistry and mechanics of frozen ground: A review, North American contribution. *Ground ice Second International Conference*. National Academy of Sciences, Washington, D.C., pp.257-288.

Anderson, D.M. and A.R. Tice 1972. Predicting unfrozen water contents in frozen soils from surface area measurements. *Highway Research Records*, **393**, pp.12-18.

Beaty, W.D., S.Clifford, P.Gogineni, B.Grimm, C.Leuschen, G.Olhoeft, K.Raney, A.Safaeinili 2001. Facility Orbital Radar Sounder Experiment for MRO 2005 (FORSE). *Report of the virtual instrument science definition team*

Berthelier, J.J., et al. 2000. The GPR experiment on NetLander. *Planetary and Space Science*, **48**, pp.1153-1159.

Bell III, J.F. and R.V. Morris, 1998. Identification of Hematite on Mars from HST. *Lunar Planet. Sci Conf., XXIX*, Houston.

Carr, M. H. 1996, *Water on Mars*. Oxford University Press.

Christensen, P.R. et al. 1999. The composition of Martian surface materials: Mars Global Surveyor thermal emission spectrometer observations. *Lunar Planet. Sci Conf., XXX*, Houston.

Christensen, P. R., et al., 2000. The distribution of crystalline hematite on Mars from the thermal emission spectrometer: Evidence for liquid water, *Lunar Planet. Sci Conf., XXXI*, Houston.

Chyba, C.F, S.J. Ostro, B.C. Edwards 1998. Radar detectability of a subsurface ocean on Europa. *ICARUS*, **134**, pp.292-302.

Clifford, S. M., and L. A. Johansen 1982. Splash craters: Evidence for the replenishment of ground ice in the equatorial region of Mars. *Lunar Planet. Sci Conf., XIII*, Houston.

Clifford, S.M 1993. A model for the hydrologic and climatic behavior of water on Mars. *J. GEOPHYS. RES.*, **98**, pp. 10973-11016.

Costard, F. 1989. The spatial distribution of volatiles in the Martian hydrolithosphere. *Earth, Moon and Planets*, **45**, pp 265-290.

Gomaa, M.M., S.A. Hussain, E.A. El-Dewany, A.E. Bayoumi 2000. The effect of texture on the electrical properties of natural hematitic sandstone in the frequency domain. *Egypt. J. Physic*.

Gooding, J.L. 1992. Soil mineralogy and chemistry on Mars: possible clues from salts and clays in SNC meteorites. *ICARUS*, **99**, pp. 28-41.

Hargraves, R.B, D.W. Collinson, R.E. Arvidson, and C.R. Spitzer 1977. TheViking magnetic properties experiments: Primary mission results. *J. Geophys. Res.*, **82**, pp. 4547-4558.

Heggy, E., P. Paillou, G. Ruffié, J.-M. Malézieux, G. Grandjean, F. Costard 2000. Dielectric measurements of volcanic materials applied to subsurface sounding of Mars. *EGS'00*, Nice, France.

Hviid, S. F. et al., 1997. Magnetic properties experiments on the Mars Pathfinder lander: Preliminary results. *Science*, **278**, pp.1768-1770.

Johari, G.P. and P.A. Charette 1975. The permittivity and attenuation in polycrystalline and single-crystal ice at 35 and 60 MHz. *J. Glaciol.*, **14**, pp. 293-303.

Konrad, J.-M. and C. Duquennoi. 1993. A model for water transport and ice lensing in freezing soils. *Water Resources Research*, **29**, pp.3109-3124.

Kuzmin, R.O., N. N. Bobina, E.V. Zabalueva, V.P. Shashkina 1988. Structure inhomogeneities of the Martian cryolithosphere. *Solar Syst. Res., XXII*, pp.195-212.

McEwen, A. et al 1999. Stratigraphy of the upper crust of Mars. *5th International Conference on Mars*, Pasadena.

Malin, M. C., K. S. Edgett, M. H. Carr, G. E. Danielson, M. E. Davies, W. K. Hartmann, A. P. Ingersoll, P. B. James, H. Masursky, A. S. McEwen, L. A. Soderblom, P. Thomas, J. Veverka, M. A. Caplinger, M. A. Ravine, T. A. Soulanille, and J. L. Warren, *P479-03, NASA's Planetary Photojournal (http://photojournal.jpl.nasa.gov/)*, 1998-13-8.

Malin, M.C and K.S Edgett 2000a. Sedimentary Rocks of early Mars. *Science*, **290**, pp.1927-1937.

Malin, M.C and K.S Edgett 2000b. Evidence for recent groundwater seepage and surface runoff on Mars. *Science*, **288**, pp. 2330-2335.

Malin, M. C., K. S. Edgett, M. H. Carr, G. E. Danielson, M. E. Davies, W. K. Hartmann, A. P. Ingersoll, P. B. James, H. Masursky, A. S. McEwen, L. A. Soderblom, P. Thomas, J. Veverka, M. A. Caplinger, M. A. Ravine, T. A. Soulanille, and J. L. Warren, *MOC2-237, NASA's Planetary Photojournal (http://photojournal.jpl.nasa.gov/)*, 2000c-06-22.

Newsom, H. E. and J. J. Hagerty 1999. Mixed hydrothermal fluids and the origin of the Martian soil. *J. Geophys. Res.*, **104**, pp. 8717-8728.

Olhoeft, G. R. 1998. Ground penetrating Radar on Mars. *7th int. Conference on GPR*, Lawrence, USA.

Olhoeft, G.R. 1991. Magnetic and electrical properties of Martian particles, sand and dust on Mars. *NASA CP-10074*, pp. 44.

Olhoeft, G.R. and D.E. Capron 1994. Petrophysical causes of electromagnetic dispersion. *5th international conference on Ground Penetrating Radar*, Proceedings, pp. 26-29.

Ori, G.G. and F. Ogliani 1996. Potentiality of the ground-penetrating radar for the analysis of the stratigraphy and sedimentology of Mars. *Planetary and Space Science*, **44**, pp. 1303-1315.

Paillou, P., G. Grandjean, J.M. Malezieux, G. Ruffie, E. Heggy, D. Piponnier, P. Dubois, J. Achache 2001. Performances of ground penetrating radars in arid volcanic regions: Consequences for Mars subsurface exploration. *Geophysical Research Letters*, **28**, pp911-914.

Picardi, G., et al. 1999. The Mars advanced radar for subsurface and ionosphere sounding (MARSIS) in the MARS EXPRESS mission. *Int. Conf. on Mars Exploration Program and Sample Return Missions*, Paris, France.

Pinet, P. and S. Chevrel 1990. Spectral identification of geological units on the surface of Mars related to the presence of silicates from earth based near infrared telescopic CCD imaging. *J. Geophys. Res.*, **95**, pp. 14435-14446.

Watts, R.D. and A.W., England 1976. Radio-Echo sounding of temperate glaciers: Ice properties and sounder design criteria. *J. Glaciol.*, **17**, pp39-49.

Reider, R.H., T. Economou, H. Wanke, A. Turkevich, J. Crisp, J. Bruckner, G. Dreibus, H.Y. McSween Jr. 1997. The chemical composition of the Martian soil and rocks returned by the mobile alpha proton X-ray spectrometer: Preliminary results from the X-ray mode. *Science*, **278**, pp.1771-1774.

Thompson, T.W., J.J. Plaut, R.E. Arvidson, P. Paillou 2000. Orbital Synthetic Aperture Radar (SAR) for Mars Post Sample Return Exploration. *Lunar Planet. Sci Conf., XXXI*, Houston.

Ulab, F. T., R. K. Moore, A. K. Fung 1982. *Microwave Remote Sensing (vol. II)*. *Artech House*, Norwood MA.

Vaughan, D.G., F.J. Hugh, C. Corr, S.M. Doake, E.D. Waddington 1999. Distortion of isochronous layers in ice revealed by ground-penetrating radar. *Nature*, **398**, pp. 323-326.

Element	XRF Viking[1]	APXS Pathfinder[2]	Djibouti basalt βs_I[3]
SiO_2	44.5	55.5	45.09
Fe_2O_3	17.4	13.1	17.74
Al_2O_3	7.15	9.1	12.98
MgO	6	5.9	5.73
CaO	5.7	6.1	9.58
TiO_2	0.58	0.8	3.72
K_2O	< 0.5	0.8	0.31
MnO	-	0.4	0.26
Na_2O	-	1.7	2.79
SO_3	-	3.2	-
Total (%)	81.8	96.6	98.2

Table I: The Average percent chemical composition of Martian and Djiboutian basalts, [1]after Clark et al. 1982, [2]after Rieder et al. 1997, [3]after F. Gasse et al.1987. We can note the excellent chemical composition match between the Djiboutian basalt and the Viking and pathfinder results. (Paillou et al, 2001)

Geological layer	Depth (m)	Sample composition	Porosity (%)	ρ ** g/cm^3	T(K)	Type of sample	Type of cell used
Dust	0-10	hematite + maghemite + basalt	50	2.7	230	Powder	Open
Basalt altered rock	10-50	80% basalt + 20% hematite	30	2.3	230	Pellet	capacitive
		80% basalt + 20% maghemite		2.5			
Lava + regolith	50-200	basalt machined pellet	30	2.2	230	Pellet	capacitive
Sedimentary deposits	200-400	compacted powder of Nakhla	30	2.1*	230	Pellet	capacitive
Basaltic regolith with ice	400-2500	80% basalt + 20% H_2O (ice)	25	2*	243	Pellet	capacitive
Basaltic regolith with water	> 2500	80% basalt + 20% H_2O (water)	20	2*	273	Pellet	capacitive

Table II: Description of laboratory samples and corresponding subsurface geological layers given by the Clifford assumed model of the Martian subsurface in Fig.3. The samples porosity and temperature used here fit with the exponentially decreasing modeled values reported by Clifford (Clifford, 1993).

* Measured by other methods then the mercury porisimeter.

** The measured bulk density

Sample	T = 300 K	T = 230 K
Basalt	$\varepsilon' = 3.2$; $\varepsilon'' = 0.18$	$\varepsilon' = 3.0$; $\varepsilon'' = 0.15$
Hematite	$\varepsilon' = 7.0$; $\varepsilon'' = 1.11$	$\varepsilon' = 6.9$; $\varepsilon'' = 1.02$
Maghemite	$\varepsilon' = 9.4$; $\varepsilon'' = 1.02$	$\varepsilon' = 9.2$; $\varepsilon'' = 0.92$
Silica	$\varepsilon' = 2.0$; $\varepsilon'' = 0.001$	$\varepsilon' = 1.5$; $\varepsilon'' = 0.001$
Gypsum	$\varepsilon' = 3.4$; $\varepsilon'' = 0.50$	$\varepsilon' = 3.2$; $\varepsilon'' = 0.43$

Table III: Temperature effect on the complex permittivity at 2 MHz for various geological materials (non compacted powder, porosity of 50%). As shown in this table there is no significant observed effect on the dielectric constant due to temperature variation.

		Measured values		Previously used values		
Geological layer	Depth (m)	ε'	tg δ	ε'	tg δ	α (dB m^{-1})
Dust layer	0-10	3-9	0.06-0.15	1-4	0.01-0.05	0.0025-0.01
Basalt altered rock	10-50	15-25	0.1-0.9	3-9	0.01-0.1	0.009-0.1
Lava + regolith	50-200	12	0.1	3-8	0.05-0.1	0.008
Sedimentary deposits	200-400	5	0.15	3-5	0.001-0.05	0.0075
Basaltic regolith with ice	400-2500	6	0.05	4-7	0.005-0.05	0.003
Basaltic regolith with water	> 2500	36	0.3	20	0.2-0.3	0.04

Table IV: Electrical properties of the Martian subsurface layers derived from terrestrials analogues at 2 MHz, compared to previously used values. α is the attenuation factor computed from our results for a one way propagation. Ranges for ε' and tg δ correspond to various concentration of iron oxide. We can note the difference between our results and the previously used values for the first three layers which are mainly constituted of volcanic materials.

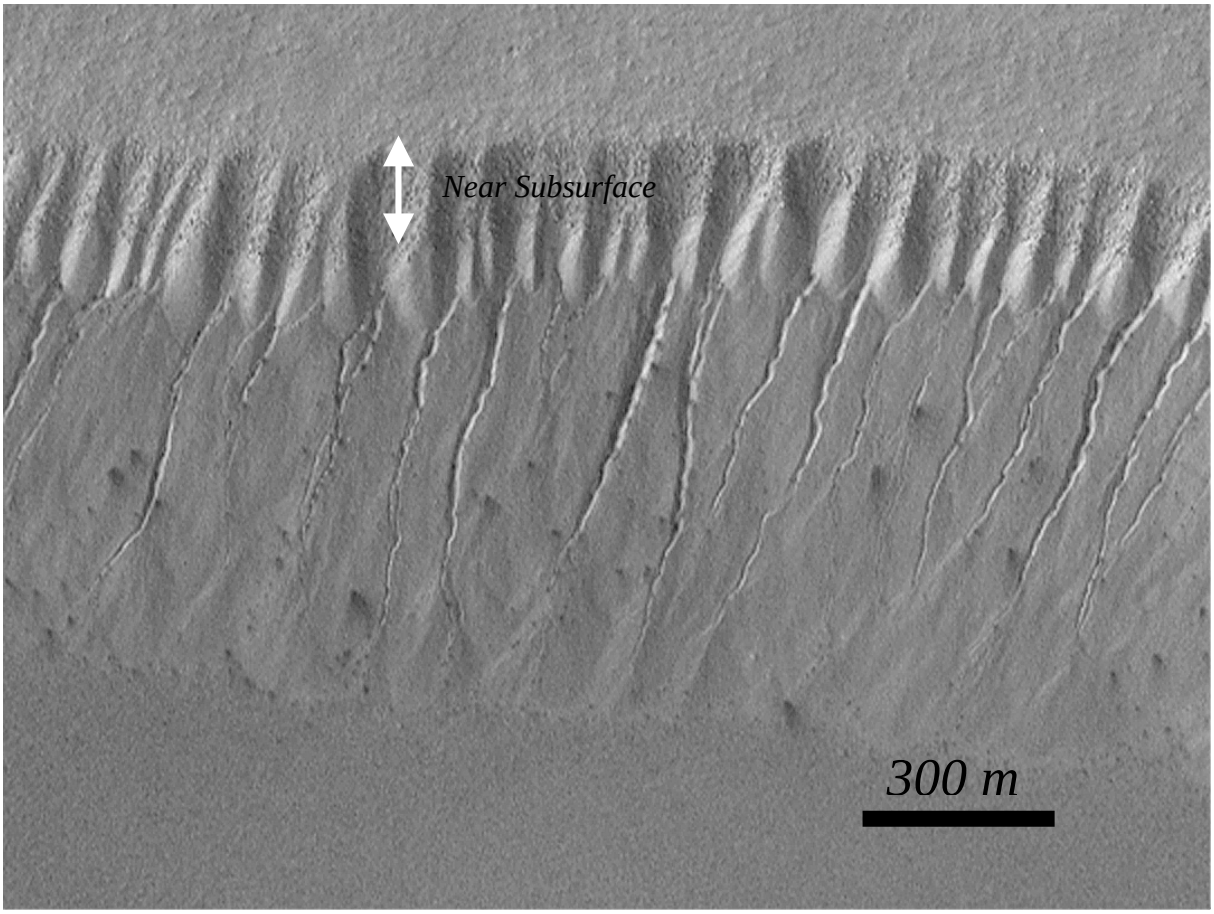

Fig.1: Observed Gullies with very sharp and deep v-shaped channels are a strong evidence for recent liquid water runoff on Mars outgoing from an ice rich layer in the near subsurface on polar pit walls (Malin et al., 2000c). We can note in the upper part of the image, the presence of a dark layer, which probably correspond to the volcanic layers constituting the near subsurface rich iron oxides materials described in table 4 and shown in Fig.3.

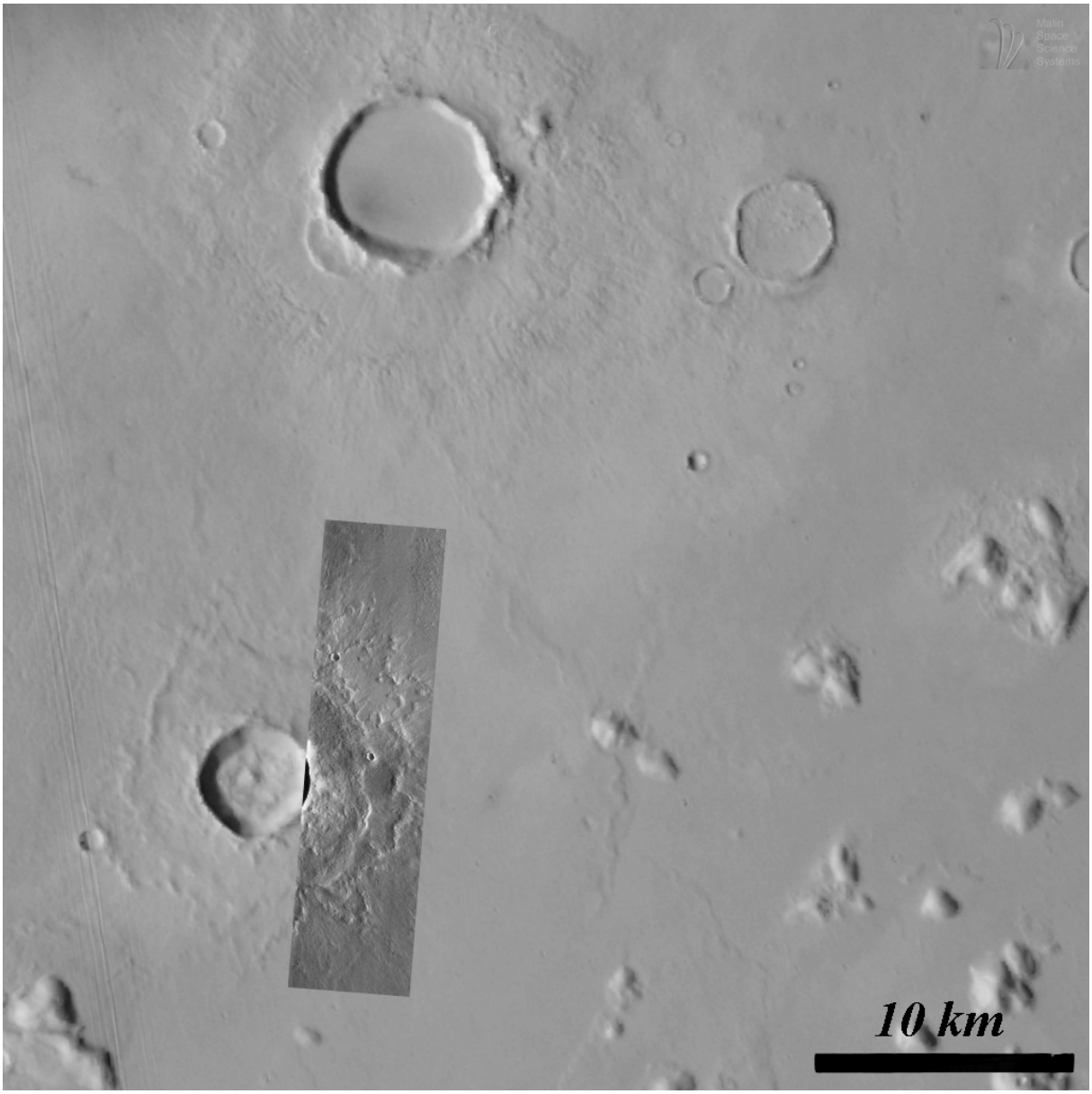

Fig.2: Double-layer rampart crater is shown within the contrasted band at the image bottom (Malin et al., 1998). The fluidized form of the ground ejected materials (ejecta) confirms the presence of a layer of ground ice in the deep subsurface that may contain liquid water at a depth where the geothermal conditions reach the second point of water shown in Fig.3.

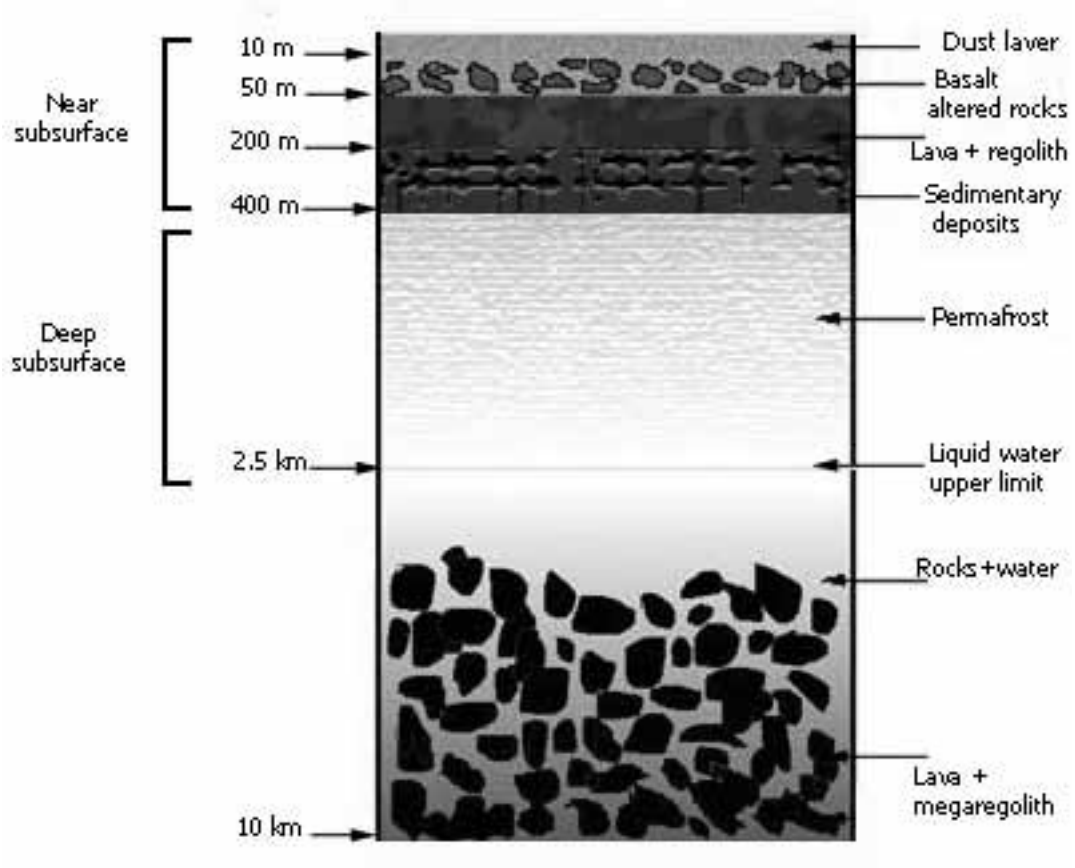

Fig.3: The Assumed Martian subsurface profile after Clifford. The near subsurface is mainly constituted of volcanic materials covered by a thin homogenous dust layer containing a considerable amount of conducting phase materials. Unlike the near subsurface, the deep subsurface should contain temperate ground ice which is relatively more resistive than the rocks constituting the near subsurface layers.

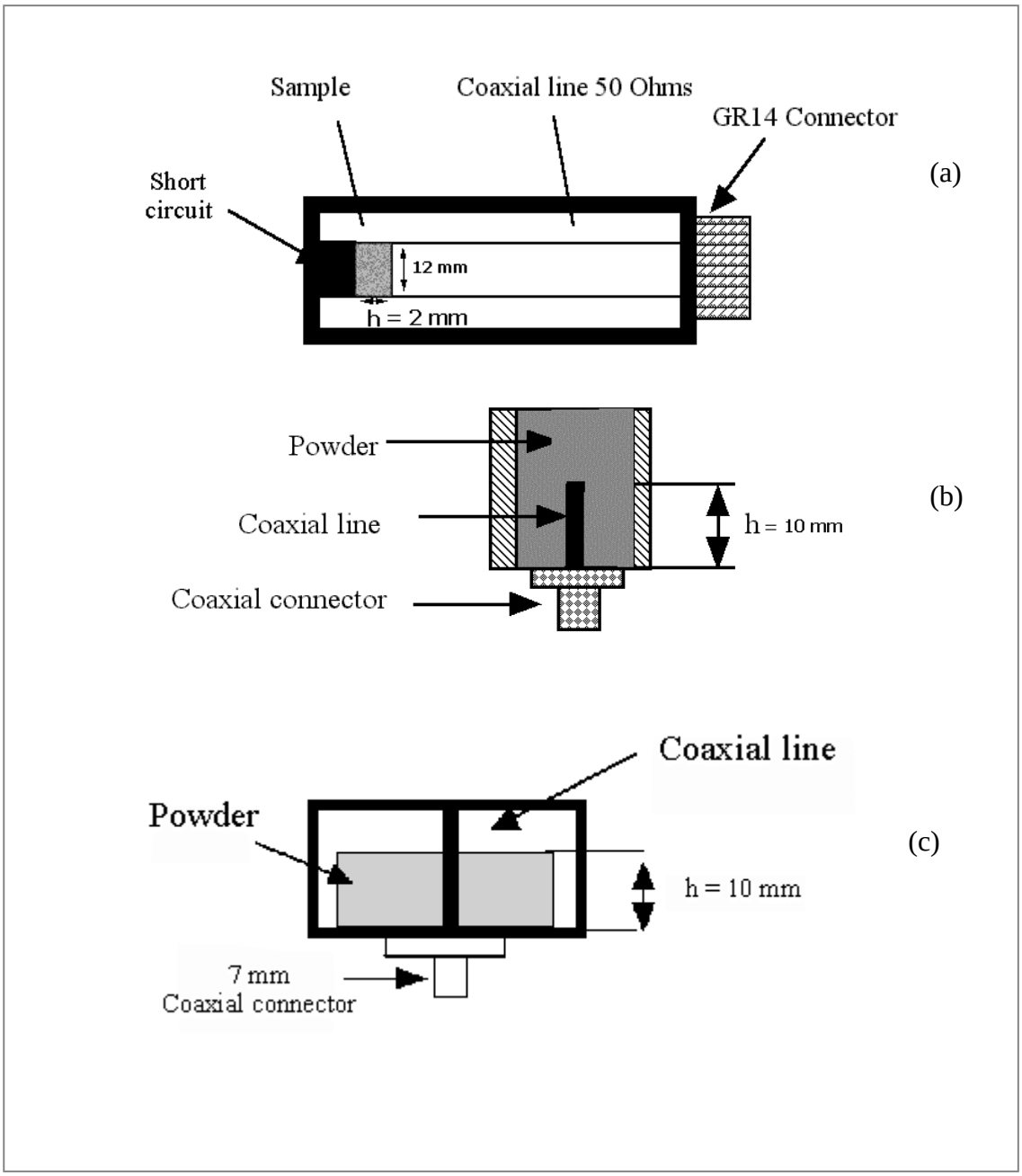

Fig.4: The three types of measuring cells used in the samples electromagnetic characterization procedure: (a) The pellet capacitive cell used to measure the permittivity of compacted and machined samples. (b) The open coaxial cell used also to evaluate the permittivity, only for powder reduced samples. (c) The magnetic cell HP1645A was used to determine the permeability of rich iron oxides powder materials. In this figure h denote the sample thickness.

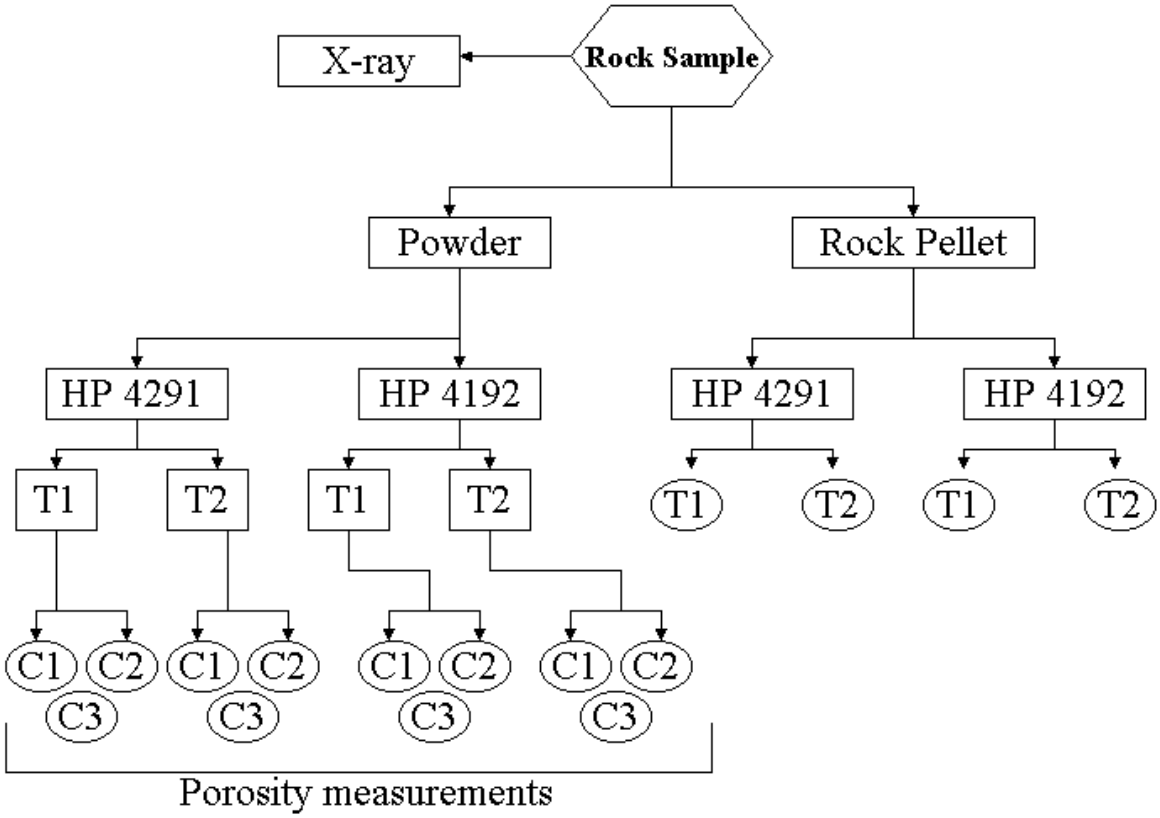

Fig.5: Sketch resuming our experimental setup. T1 and T2 are two temperature respectively 230 K and 300 K, those two temperature levels allowed us to evaluate the variation of the dielectric constant as a function of temperature, results are shown in table 3. C1, C2 and C3 are three different compaction levels (C1<C2<C3) corresponding to the subsurface layers described in table 2 and shown in fig.3 (starting from 50 to 2500m) measured using the capacitive pellet cell ((a) fig.4). To simulate the surface, we used powder measurements at 230 K (T1) with the open cell ((b) fig.4). Electromagnetic properties of samples were measured using the two analyzers HP4291A and HP4192A to avoid measurements errors in their band limits. Porosity measurements were done at the end of the experimental procedure to avoid mercury contamination of samples while performing the electromagnetic characterization.

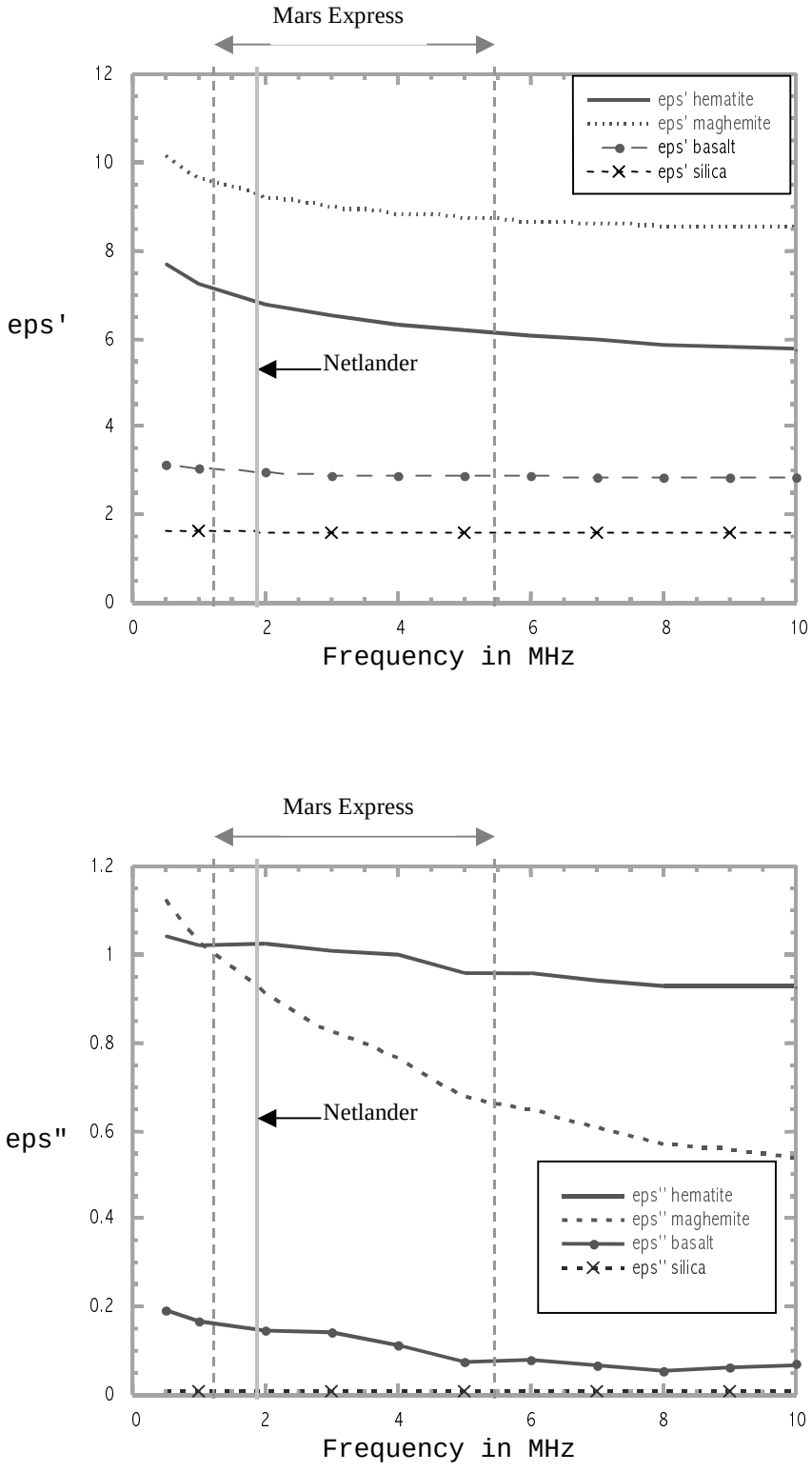

Fig.6: Dielectric constant for non-compacted volcanic materials (porosity of 50% corresponding to a bulk density $\rho = 2.7$ g/cm^3) constituting the Martian dust layer: real part (top) and imaginary part (bottom).

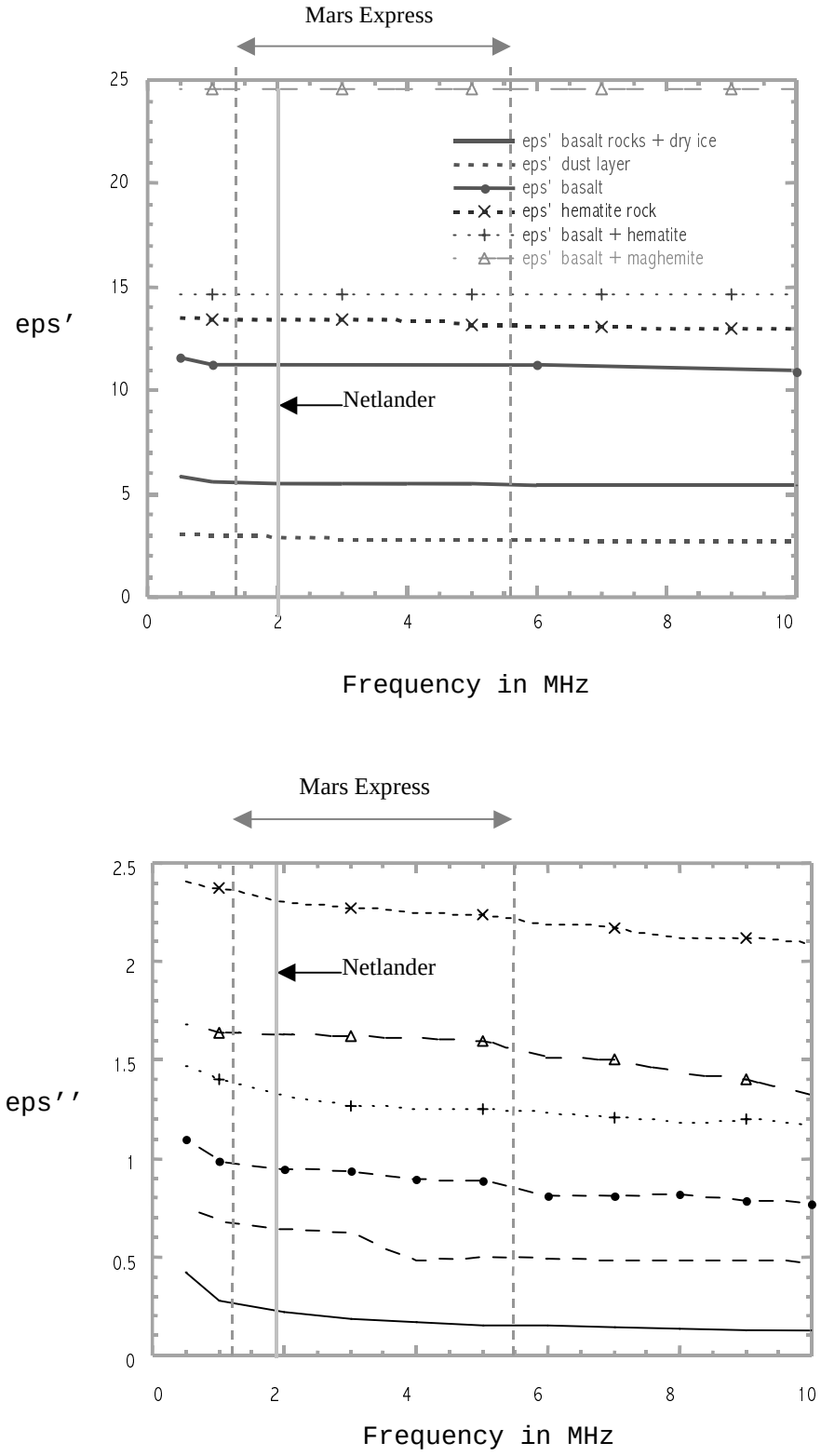

Fig.7: Dielectric constant for compacted volcanic materials, constituting the Martian subsurface layers: real part (top) and imaginary part (bottom).

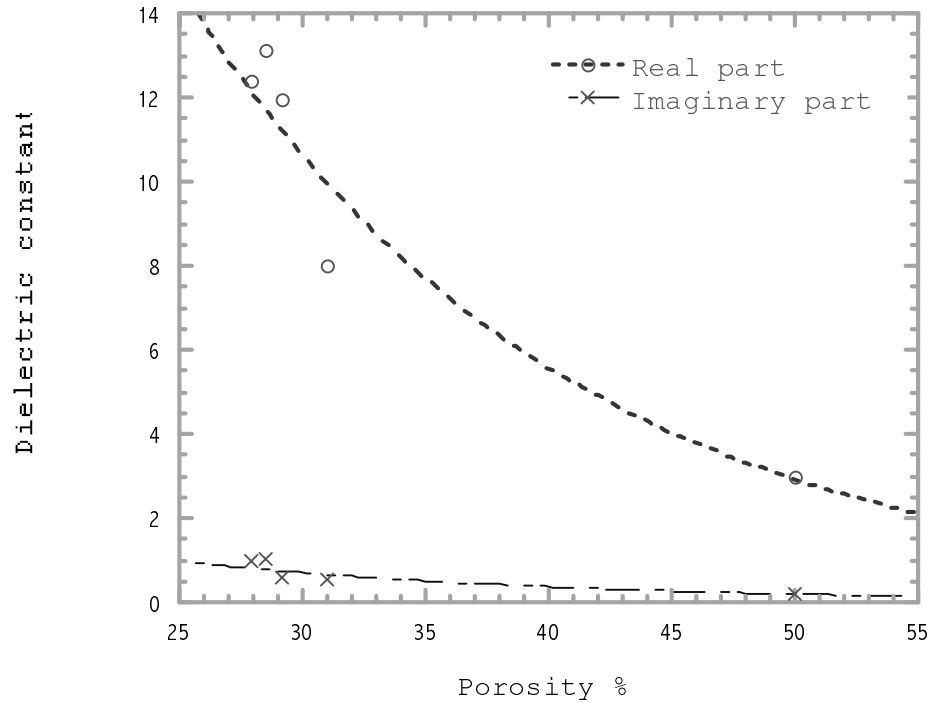

Fig.8: Variations of the real and imaginary part of the dielectric constant with respect to the porosity for the Djiboutian basalt, at a frequency of 2 MHz. (The dotted lines represent the exponential regression of the measured points)

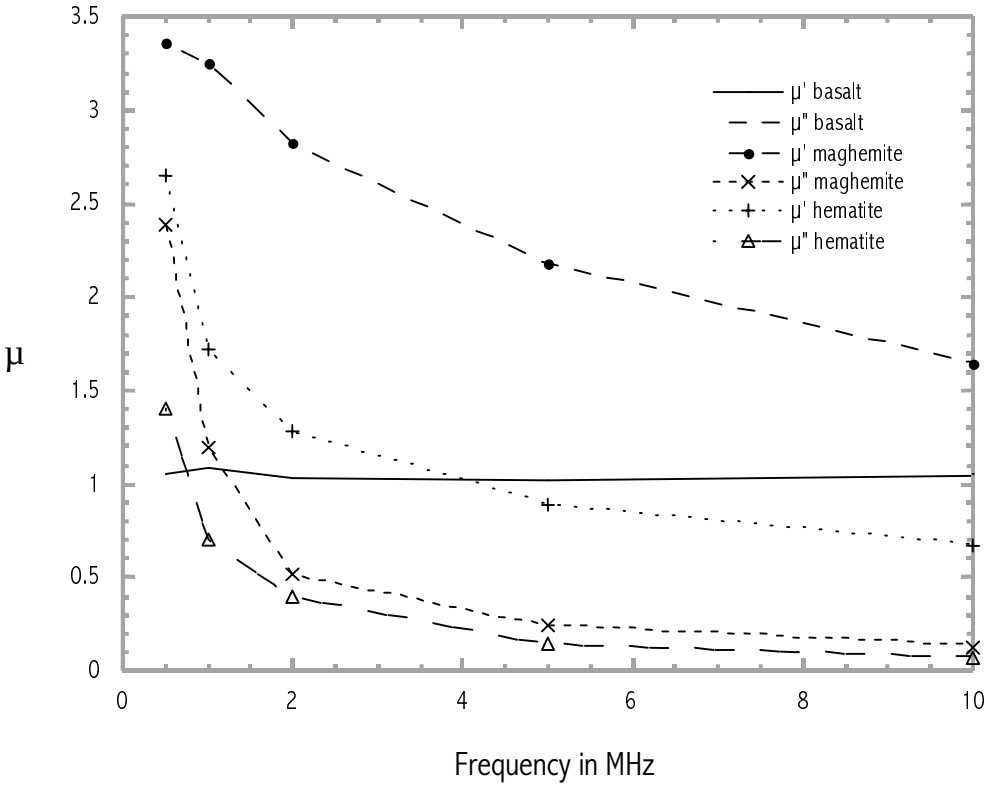

Fig.9: Laboratory measurements of the magnetic properties of the more probable iron oxide rich materials constituting the Martian surface and near subsurface layers.

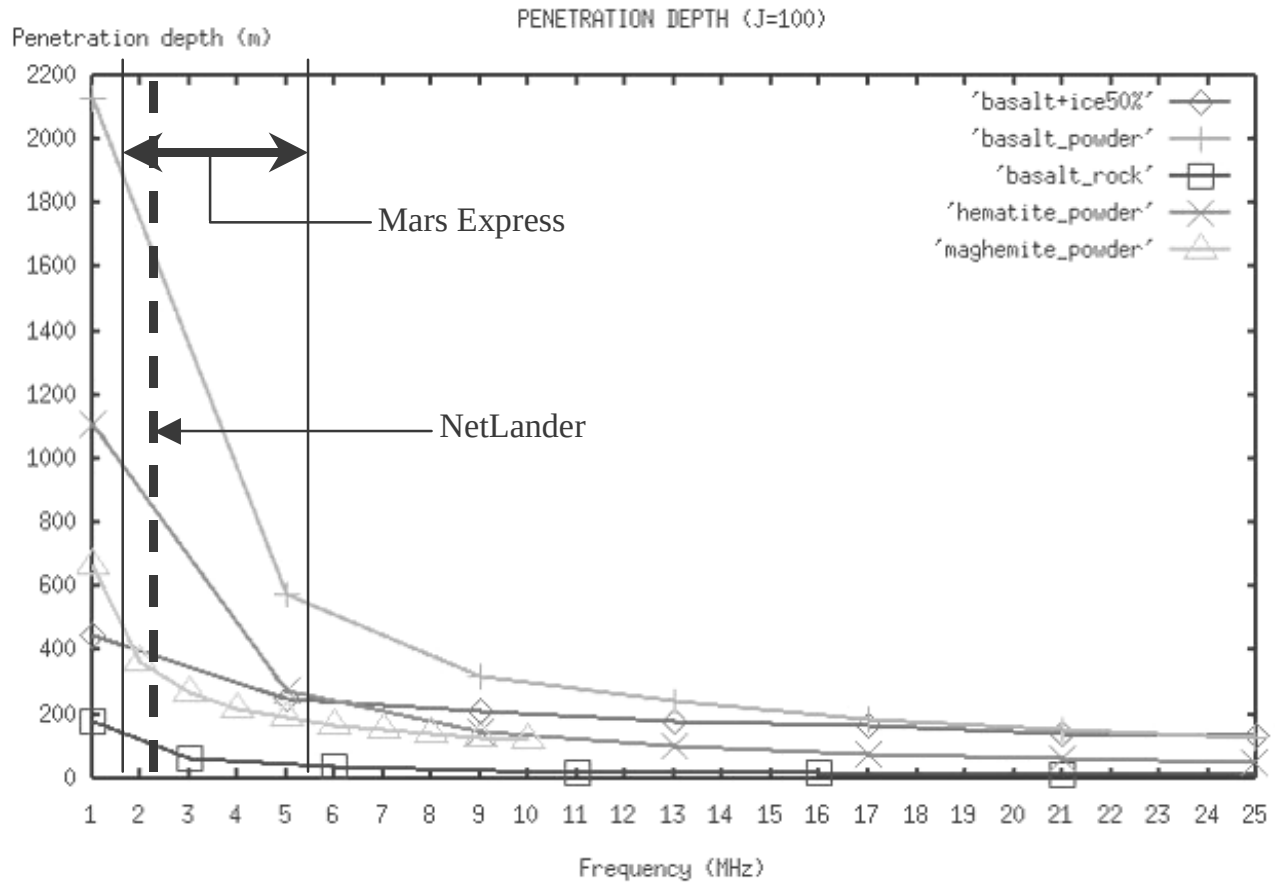

Fig.10: The penetration depth δ_p for Martian most common surface and subsurface materials (attenuation factor J=100). We can clearly note that penetration depth vary exponentially at the low frequency sounding band from 1 to 6 MHz while it show linear behaviour for higher frequency. Those results do not take in consideration the surface reflection that can significantly decrease the penetration depth for Mars Express MARSIS instrument.

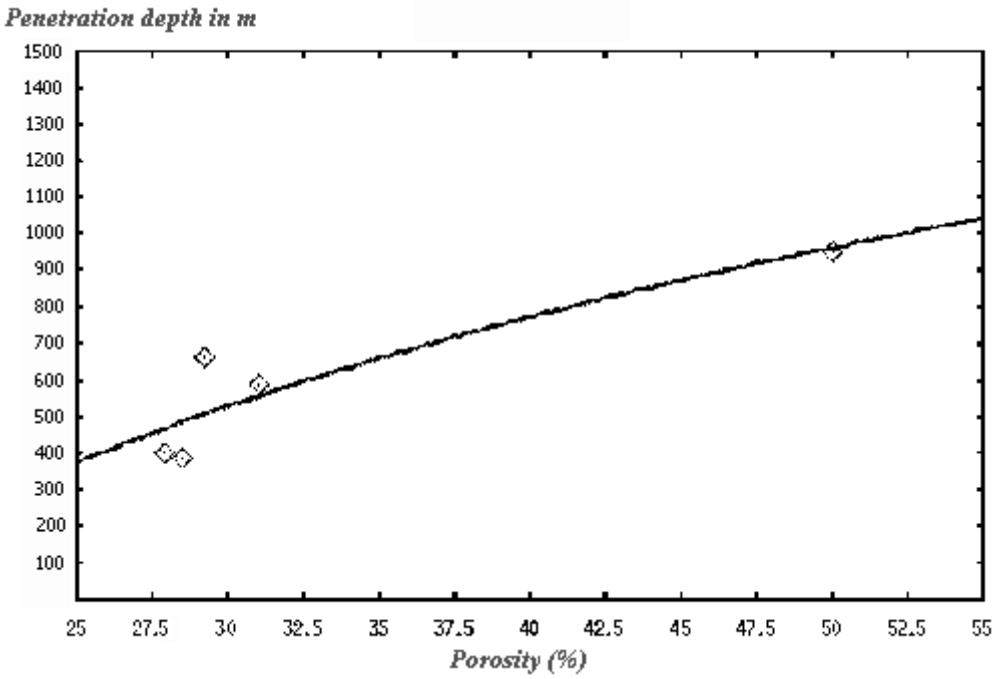

Fig.11: Penetration depth δ_p as a function of the porosity for Djiboutian basalt at 2 MHz. We can observe the quasi-linear dependency between δ_p and the porosity. This show the impact of porosity that we take into consideration when we evaluated the assumed Martian subsurface dielectric profile. The slope of the curve is a characteristic of the material being used and the sounding frequency.

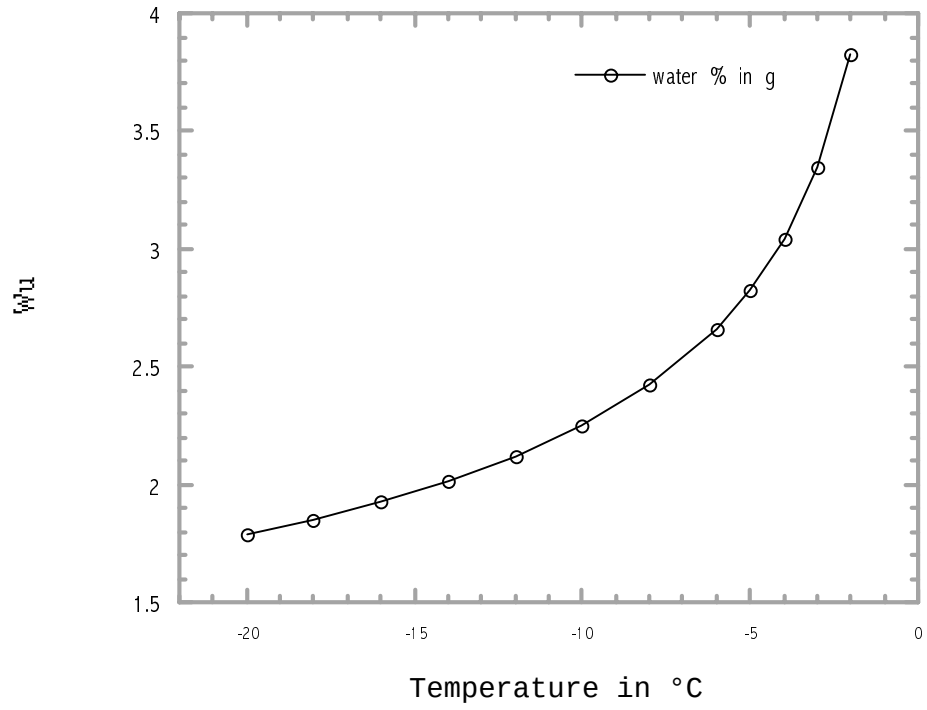

Fig.12: Variation of the amount of unfrozen water (weight percent in one gram) as a function of the ground temperature for porous frozen basalt.